DOI: 10.1177/1099636218760307

Quasi-static and fatigue properties of a balsa cored sandwich structure with thermoplastic skins reinforced by flax fibres

Arthur Monti[1], Abderrahim EL Mahi[1], Zouhaier Jendli[2] and Laurent Guillaumat[3]

Abstract

This paper presents the results of several experimental analyses performed on a bio-based sandwich structure. The material studied is made up of thermoplastic skins reinforced by flax fibres and applied to a balsa core. It is produced by a single-step liquid resin infusion process. First, the skin–core interfacial properties were measured and compared with those of the existing materials. Then, several quasi-static and dynamic analyses were performed to study the flexural behaviour of sandwich beams. The elastic and ultimate properties of the skins and core were deduced from these flexural tests. In addition, a failure mode map was developed based on the existing theories to explain the failure modes observed under different boundary conditions. The influence of the statistical spread of the core's mechanical properties on the failure of sandwich beams was considered. Moreover, fatigue analyses were conducted to determine the fatigue resistance of this bio-based structure. Its behaviour was compared with that of the previously tested non-bio-based sandwich beams.

[1]LAUM – Laboratoire d'Acoustique de l'Université du Maine, Avenue Olivier Messiaen, France
[2]ESTACA'Lab – Pôle Mécanique des Matériaux Composites et Environnement, Parc Universitaire Laval-Changé, Rue Georges Charpak, France
[3]LAMPA – Laboratoire Angevin de Mécanique Procédés et innovAtion, Arts et Métiers ParisTech Campus Angers 2, France

Corresponding author:
Arthur Monti, LAUM – Laboratoire d'Acoustique de l'Universite du Maine, Avenue Olivier Messiaen, 72085 Cedex 9 Le Mans, France.
Email: arthur.monti.etu@univ-lemans.fr

Finally, the fatigue loss factor evolution of this structure under several loading ratios was measured and discussed. This study aims to determine some of the main mechanical properties of this material to see whether or not it might be suitable for industrial applications currently using glass fibre reinforced polymer/foam cored sandwich structures.

Keywords
Sandwich structures, flexural properties, flax fibres, fatigue, thermoplastic

Introduction

In recent years, bio-based composites have become a subject of interest in composite research and in numerous industrial fields [1–4]. To reduce the environmental impact while providing high technical properties, the use of vegetal fibre reinforced polymers (VFRP) is being widely studied. Plenty of research work has already proven that such materials may be suitable for industrial applications that currently use glass fibre reinforced polymers (GFRP) [5,6]. Moreover, thermoplastic composites are also widely being studied because they allow the recycling of composite materials – a significant aspect of the end of life management of traditional thermoset composites. As a consequence, potentially recyclable bio-based sandwich structures may be serious contenders to face further industrial challenges. Sandwich materials are usually made of a light core inserted between stiff and resistant skins. This increases the quadratic moment of the structure, resulting in very high stiffness and strength with minimal impact on the mass. Although the number of research projects appears to be smaller concerning bio-based sandwiches than bio-based composites, several authors have already studied such materials and revealed interesting physical properties. Mancuso et al. [7] recently presented a flexural analysis of a green sandwich composite of flax fibre reinforced facings and cork core. They discussed the influence of three different manufacturing techniques. Cork appears indeed to be often studied as a core material [8,9]. One of its main advantages is its ability to absorb energy. Balsa wood is also among the most frequently studied bio-based cores due to its high specific compressive and shear properties [10–12]. It has often been used in marine applications reinforced with GFRP [13]. Le Duigou et al. [14] have studied a fully bio-based sandwich made of polylactic acid (PLLA)/flax skins and a balsa core manufactured in a single-step thermocompression process. They achieved good mechanical properties and proved that the manufacturing of this material had a lower environmental impact than sandwiches with GFRP skins. Karaduman et al. [15] also studied the flexural properties of a sandwich beam made up of lute/

polypropylene (PP) skins and a balsa wood core. The authors emphasised the higher mechanical stiffness and strength of the balsa core compared to polyethylene terephthalate (PET) foam or PP honeycomb cores. In addition to its good specific properties, balsa wood has also been studied and used a lot because of other interesting properties. Kandare et al. [16] have emphasised the interesting fire reaction of a balsa cored structure with skins made of flax/epoxy. Moreover, several studies prove that the use of natural materials in sandwich structures may result in enhanced vibration damping properties [17,18].

In this context, the present paper focuses on the experimental quasi-static and fatigue characterisations of a bio-based sandwich structure made up of thermoplastic skins reinforced with flax fibres and a balsa core. This material, manufactured in a single-step liquid resin infusion process, brings new perspectives to the development of potentially recyclable bio-based structures. Thus, several mechanical tests were conducted to determine its main mechanical properties. Some of them were compared to those of traditional non-bio-based materials in order to see whether or not this material would be suitable for applications currently using GFRP/foam core sandwiches.

Experimental program

Materials and manufacturing

The reinforcement used is a 200 g/m^2 dry FlaxTape manufactured by LINEO [19]. It is composed of purely unidirectional technical and elementary flax fibres. The resin used is the innovative ELIUM RT-150 thermoplastic liquid resin produced by ARKEMA [20]. The low viscosity of this resin allows the manufacturing of thermoplastic composites with processes such as resin transfer molding, usually used for thermoset composites. In this study, sandwich structures were produced in a single-step liquid resin infusion process at room temperature, described in a previous work [18]. A typical panel obtained with this process is presented in Figure 1. BALTEK balsa panels with a density of 150 kg/m^3 were used as the core. To facilitate the resin infusion, balsa panels cut into regular elementary blocks (25 mm $\times$ 50 mm $\times$ 15.9 mm) and assembled on a thin mesh grid were used. The gaps between adjacent blocks facilitate the migration of the resin from the upper to the lower parts. These balsa panels are illustrated in Figure 2(a). One can remark that these elementary blocks are made up of several pieces of wood, coming from different trees. As a consequence, the core density is locally scattered. To quantify these variations, 50 elementary blocks were randomly extracted, measured and weighed. Figure 2(b) presents the frequency distribution histogram of these blocks. A Gaussian law with an average value of m = 150 kg/m^3 and a standard deviation of $\sigma = 27$, leading to a CoV of 18%, was used to describe this statistical spread. This high local scattering is expected to have consequences on the failure behaviour of this sandwich structure. As a matter of fact, lot of authors [21–24] have proven that the mechanical properties of balsa wood

Figure 1. Flax/Elium/Balsa sandwich panel.

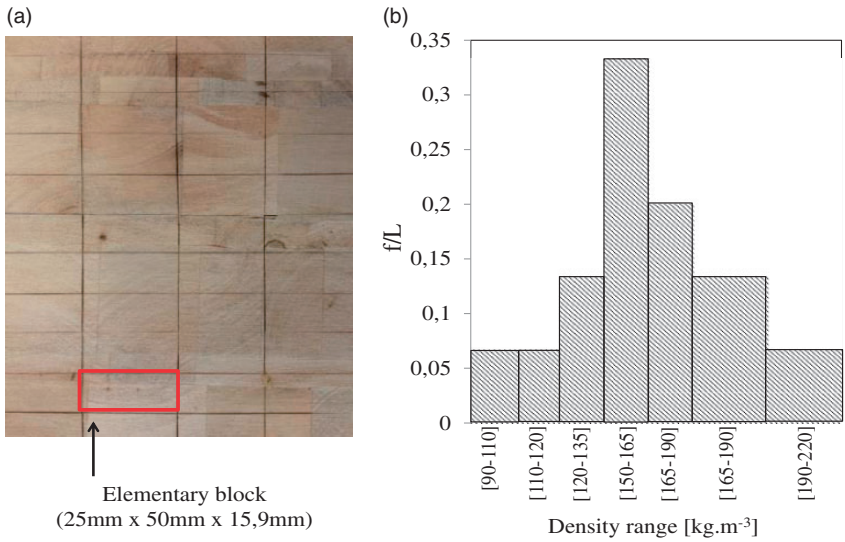

Figure 2. (a) Type of balsa core panel used; (b) statistical dispersion of the density.

closely depends on its density because of its cellular microstructure. As a consequence, these authors proposed a correlation between mechanical properties P (such as Young's or shear modulus, failure stresses, etc.) and wood density ρ with the following form

$$P = C\rho^{\alpha} \tag{1}$$

with C and α determined experimentally.

For this study, two different sets of specimen were prepared. For one of them, labelled $[0]_5$, the skins were made up of five unidirectional plies of flax, and for the other one, labelled $[0/90]_s$, the skins were made up of four plies of flax with a $[0/90]_s$ stacking sequence. Unidirectional $[0]_5$ specimens were first tested in order to achieve sufficient stiffness to observe compressive failure of the skins and core shear failure in a satisfying range of span length values. $[0/90]_s$ specimens were then tested to provide results and information concerning a common bi-directional layup more often used in numerous applications.

Skin core interface strength testing

The skin–core interfacial strength was investigated through flatwise tensile tests performed according to the ASTM C297/C297M [25] standard test method. This experimental test consists in loading sandwich square samples under stress along an axis parallel to the thickness. Five $[0/90]_s$ samples with a section of 40 mm$\times$40 mm were tested with a grip separation rate of 1 mm/min. The load was measured with a 100 kN force sensor and the displacement applied was measured with a linear variable differential transformer. The failure modes of the different specimens were analysed. Only samples exhibiting a typical skin/core interface failure mode were considered for calculating the interfacial ultimate stress.

Flexural tests

To study the flexural behaviour of this sandwich structure, three-point bending tests were performed according to the ASTM C393 and ASTM D7249 [26,27] standard test methods. First, monotonic tests were performed on two different sets of sandwich beams with a crosshead displacement speed of 5 mm/min. Then, quasi-static cyclic tests were performed to investigate the evolution of permanent damage and beam stiffness. Based on these results, $[0]_5$ and $[0/90]_s$ beams were tested in monotonic three-point bending with different span lengths in their elastic domain in order to determine the main elastic properties of the components, such as the Young's modulus of the skins and the shear modulus of the core. Finally, failure analysis was performed on $[0]_5$ specimens. The span length varied from 80 to 250 mm. Short beam tests were used to determine the shear strength of the core whereas long beams tests were used to measure the ultimate properties of the faces. Tests were repeated for each boundary condition in order to take into account the dispersion of the results due to the materials and experimental conditions. This experimental program is summarised in Table 1.

Fatigue tests

To investigate the fatigue behaviour of this sandwich structure, three-point bending dynamic cyclic tests were performed for $[0/90]_s$ specimens. Two different span lengths ($d = 110$ mm and $d = 250$ mm) were used in order to distinguish the flexural and shear dynamic behaviour. To compare the results with previous analyses

Table 1. Quasi-static flexural tests: Experimental program.

$[0]_5$	Span length (mm)	300	250	230	210	190	170	150	110	80
	No. of specimen tested	3	5 + 1[a]	5	5	5	5	5	6	5
$[0/90]_s$	Span length (mm)	300	250	230	210	190	170	150	110	80
	No. of specimen tested	3	5 + 1[a]	0	5	5	5	5	5	0

[a]Quasi-static cyclic test.

Table 2. Fatigue tests: Experimental program.

Span length (mm)	$d = 250$					$d = 110$					
Amplitude (mm)	1	1.5	2	2.5	3	0.1	0.2	0.3	0.4	0.5	0.6
r (%)	60	65	70	75	80	50	55	60	65	70	75
No. of specimen tested	3	3	3	3	3	3	3	3	3	3	3

performed in the laboratory with non-bio-based glass/epoxy/PVC foam core sandwiches, the fatigue tests were displacement-controlled with a frequency of 5 Hz. Fatigue analyses performed on flax/epoxy composites [28] and balsa cored sandwiches [29] seem to indicate that this frequency is not likely to cause a significant temperature increase in the structure. For the span length $d = 250$ mm, specimens were loaded with an average displacement D_m defined as 50% of the failure displacement under quasi-static monotonic three-point bending tests D_R. The amplitude of displacement was then varied in order to increase the loading ratio r defined by

$$r = \frac{D_{max}}{D_R} \tag{2}$$

where D_{max} is the maximum displacement applied during the cycle. For the span length $d = 110$ mm, the average displacement D_m was defined as 40% of the failure displacement, in order to avoid early core shear failure. At least three specimens per loading configuration were tested. This experimental program is summarised in Table 2, which presents the displacement amplitude applied to achieve different loading ratios.

Quasi-static analysis

Interface strength

The quality of the skin–core interface is among the first-order problems in sandwich design. The flexural properties of the complete structure rely on this

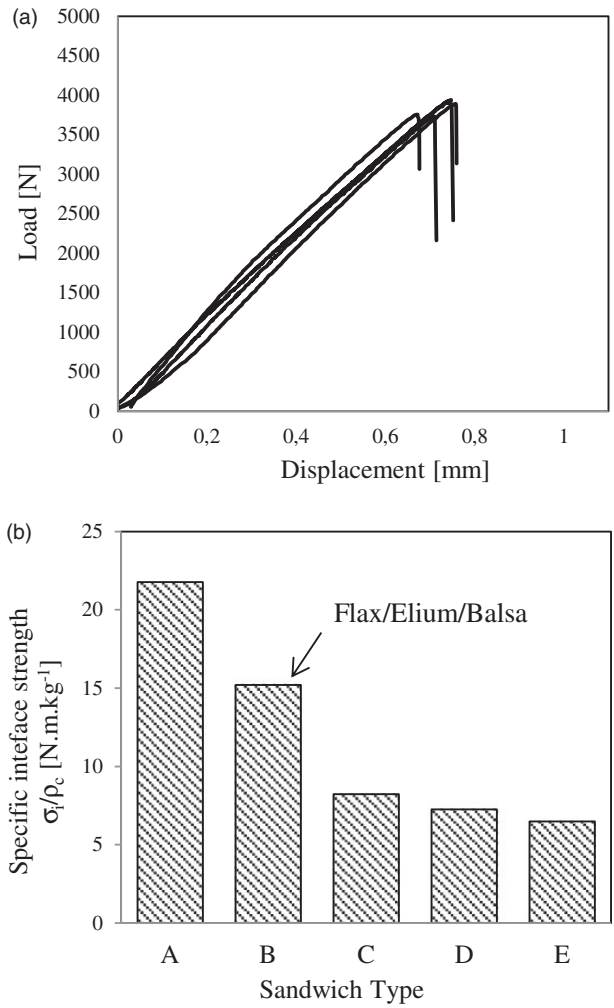

Figure 3. Flatwise tensile tests results: (a) load–displacement curves; (b) specific interfacial strength of different sandwich materials.

mechanical connection. For this reason, flatwise tensile tests were performed to measure the interfacial strength of this bio-based sandwich and to compare it to those of existing materials. The experimental load–displacement curves obtained are presented in Figure 3(a). Satisfactory repeatability is achieved, with failure load scattering that does not exceed 15%. The interfacial failure stress is shown in Table 3, which compares the results obtained with those of several authors for different kinds of sandwich materials tested in flatwise tension [30–33]. Figure 3(b) presents these failure stresses normalised by core density. The specific interfacial

Table 3. Material properties and skin–core interfacial strength of different sandwich materials.

Specimen	Skin	Core	ρ_c (kg/m^3)	σ_i (MPa)	Reference
A	Carbon Fiber/ Epoxy	Aluminum honeycomb	39.5	0.86	Hou et al.[30]
B	Flax/Elium	Balsa core	150	2.28	Experimental
C	Glass/Epoxy	PU foam	96	0.79	Tuwair et al.[31]
D	Glass/Epoxy	PP honeycomb	110	0.8	Correia et al.[32]
E	Carbon/Epoxy	PU foam	160	1.04	Sok et al.[33]

strength of the Flax/Elium/Balsa sandwich appears to be very promising, compared to PVC foam sandwiches. There may be at least two reasons to justify these good interfacial properties. First, the gaps between adjacent balsa wood blocks, visible in Figure 2(a), result in a regular pattern of resin inside the core which certainly contributes to the skin–core interface quality. Then, the open cell configuration of the core allows the absorption of a certain amount of resin. Due to the low viscosity of the resin, which can penetrate the larger pores, mechanical anchoring is created between the skins and the core. This phenomenon has been described by Le Duigou et al. [14] by means of X-ray tomography analyses of PLLA/Flax/Balsa sandwich structures.

Flexural properties of sandwich beams and elastic properties of their components

As sandwich structures are mainly subjected to flexural loadings, different tests were conducted to investigate the flexural behaviour of Flax/Elium/Balsa sandwich beams. First, two sets of $[0]_5$ and $[0/90]_s$ beams were tested in three-point bending with a span length of 250 mm. Figure 4(a) presents the force–displacement curves obtained. $[0]_5$ specimens appear, as expected, stiffer and more resistant due to the higher mechanical properties of the faces. Moreover, the linear elastic domain seems more pronounced. On the contrary, $[0/90]_s$ specimens exhibit a shorter elastic domain followed by a nonlinear behaviour. Figure 4(b) presents the force–displacement curves obtained for both specimens tested in quasi-static cyclic loading. Based on these results, the evolutions of the stiffness and the permanent displacement with the number of cycle were measured. These evolutions are presented in Figure 5. It is worth noting that for both types of specimen, a permanent displacement is observed after the second cycle, associated with a stiffness decrease. This results from the appearance and increase of damage mechanisms in the structure. The irreversible displacement measured may also be attributed to the plastic behaviour of the Flax/Elium thermoplastic composite skins.

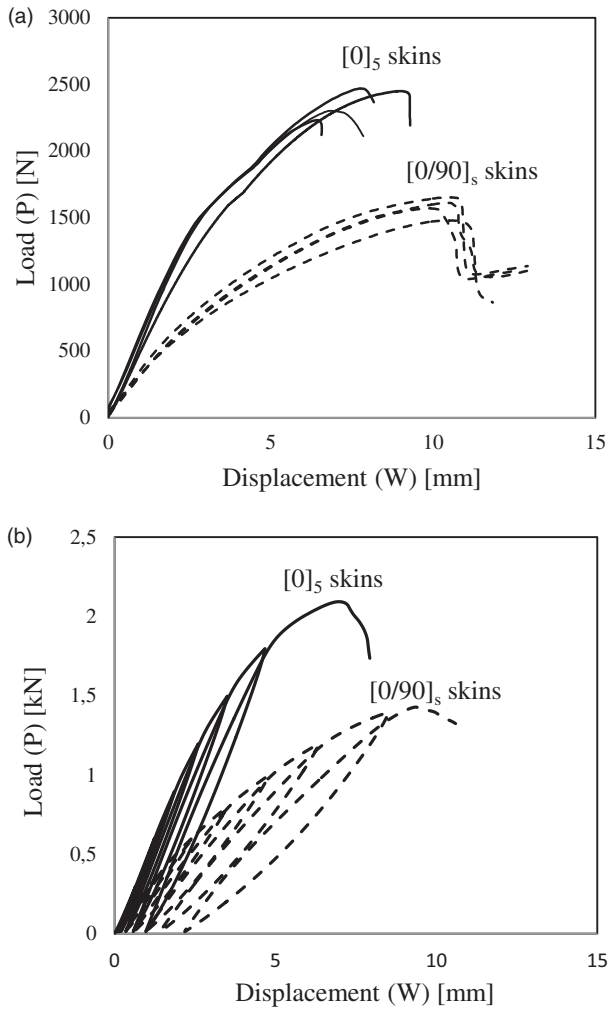

Figure 4. Quasi- tests performed on sandwich beams with two different skin configurations: (a) monotonic three-point bending; (b) quasi-static cyclic loading.

Based on these results, an elastic analysis was performed on these two different sets of sandwich beams to determine the main mechanical properties of the skins and core. Under three-points bending loadings, the relation between the applied load P and the deflection W is given by

$$\frac{W}{Pd} = \frac{d^2}{48D} + \frac{1}{4N} \tag{3}$$

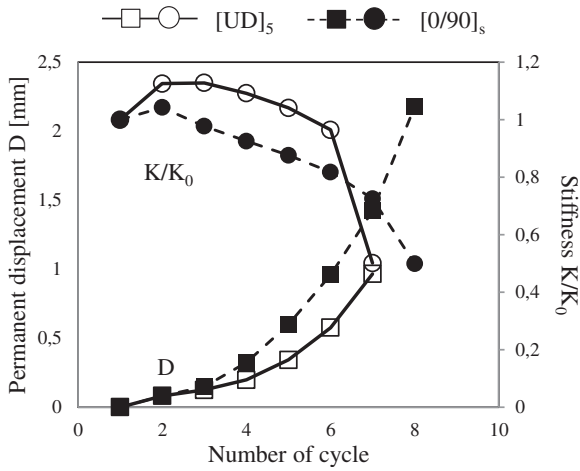

Figure 5. Evolution of the stiffness and irreversible displacement with the number of cycle.

where d is the span length, and D and N the flexural and shear rigidity of the beam. Considering a symmetrical sandwich cross section, we have

$$D = \frac{E_f t_f^3}{6} + \frac{E_f t_f h^2}{2} + \frac{E_c t_c^3}{12} = \ 2D_f + D_0 + D_c \tag{4}$$

with E_f and E_c the Young's modulus of the skins and the core, t_f and t_c their respective thickness, $h = (t_f + t_c)$, D_f the bending stiffness of the faces about their individual neutral axes, D_0 the bending stiffness of the faces about the middle axis and D_c the bending stiffness of the core. Considering the thin face and weak core approximations, respectively given by

$$\frac{2D_f}{D_0} < 0.01 \text{ and } \frac{D_c}{D_0} < 0.01 \tag{5}$$

The flexural rigidity D and shear rigidity N per unit of width of the beam can be simplified

$$D = \frac{E_f t_f h^2}{2} \text{ and } N = \frac{G_c h^2}{t_c} \tag{6}$$

Then, the span length was varied from 110 to 300 mm and the beams were tested in their elastic domains. Figure 6(a) presents the evolution of the $W/(Pd)$ ratio with respect to the square of the span length d^2. The experimental plots can be

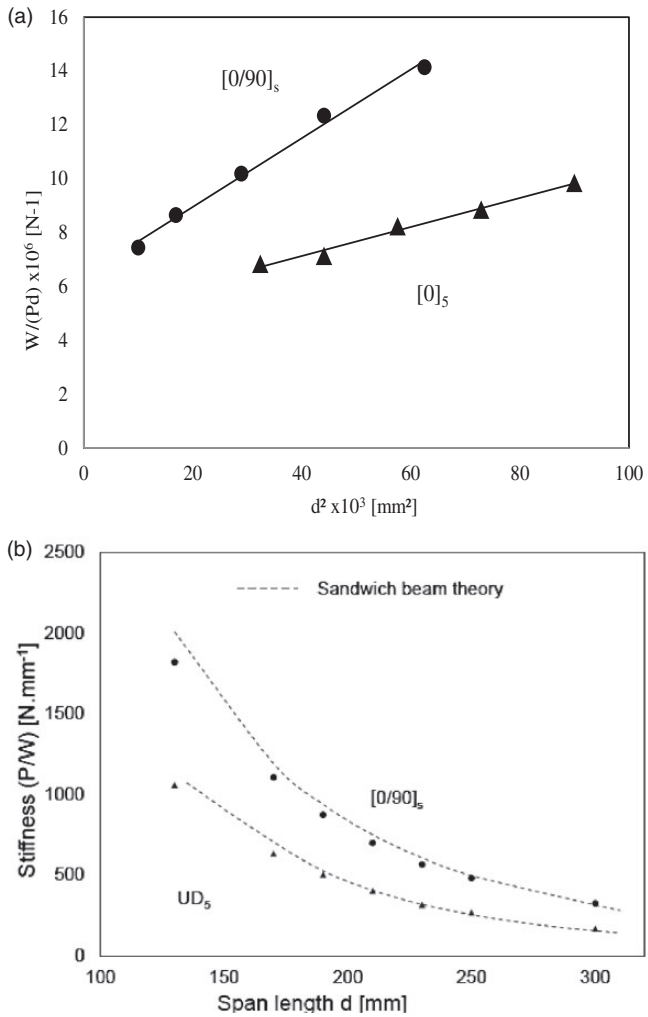

Figure 6. (a) Evolution of the ratio (w/pd) with respect to the span length in three-point bending for $[0]_5$ and $[0/90]_s$ specimens under elastic deformations; (b) comparison of the experimental results with sandwich beam theory.

fitted by a linear equation. According to equation (3), it is possible to deduce the equivalent flexural rigidity D from the slope of the linear fitting, and the shear rigidity N from the intercept. As a consequence, the Young's modulus of the Flax/Elium skins and the shear modulus of the balsa core were deduced using equation (6). The results are presented in Table 4. The Young's modulus of the skins measured for both sets of specimens are very close to the Young's moduli of unidirectional and $[0/90]_s$ Flax/Elium laminates measured

Table 4. Elastic and ultimate properties of the skins and core.

	$E_f^{[0]5}$	$\sigma_{fc}^{[0]5}$	$E_f^{[0/90]s}$	$\sigma_{fc}^{[0/90]s}$	G_c	τ_c
Unit	GPa	MPa	GPa	MPa	MPa	MPa
Average	24	120	11	90	225	2.5
Standard deviation	1.3	8	1.4	7	48	0.5

in previous studies [18,34]. On the other hand, the shear modulus of the core appears to be 25% higher than the modulus announced by the manufacturer and measured according to ASTM C273 test method [35]. This may be explained by the contribution of the skins' shear properties, as well as a contribution of a certain amount of resin trapped in the core, particularly in the gaps between adjacent balsa blocks. Figure 6(b) presents a comparison of the experimental results with the analytical theory presented in the previous section. A satisfying correlation is achieved for both specimens.

Failure analysis

To determine the flexural and shear ultimate properties of the sandwich beams, monotonic three-point bending tests were performed on $[0]_5$ specimens with different span lengths. At least five beams were tested to failure for every boundary condition. A high-speed digital camera was used to record the failure of every specimen and identify the failure modes. Depending on the span length, two major failure modes were identified. For the longest beams, a compressive failure of the upper skin was observed, whereas for the shortest beam, a core shear failure of the core occurred. These failure modes are illustrated in Figure 7. In some cases for the shortest span length, local indentation of the core was observed below the upper span. These specimens were ignored for the rest of the analysis. Then, the compressive failure stress σ_{pc} of the upper skin was estimated by

$$\sigma_{pc} = \frac{Pd}{2t_f b(t_s + t_c)} \tag{7}$$

where t_s is the global thickness and b the width of the beam. Moreover, the core shear stress τ_c was calculated using

$$\tau_c = \frac{P}{b(t_s + t_c)} \tag{8}$$

The results obtained are presented in Table 4. Moreover, the failure stresses measured for every specimen, normalised by the average compressive or shear failure stress are shown in Figure 8. This figure also indicates the failure mode observed. It is worth noting that the statistical spread of the results seems to

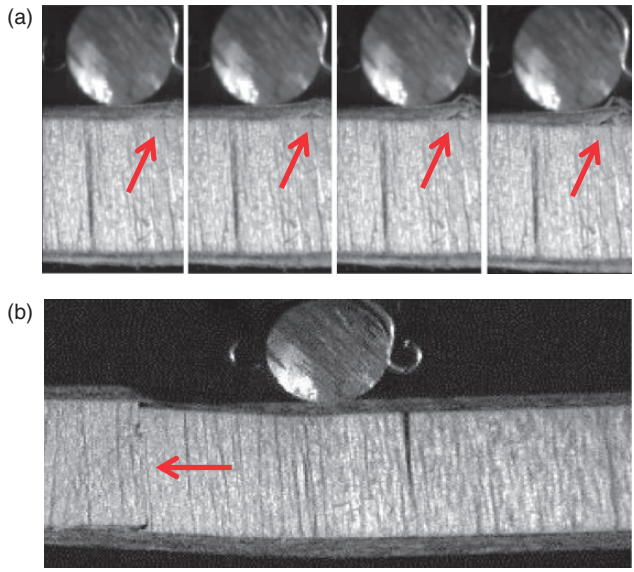

Figure 7. Main failure modes observed: (a) compressive failure of superior skins; (b) core shear failure.

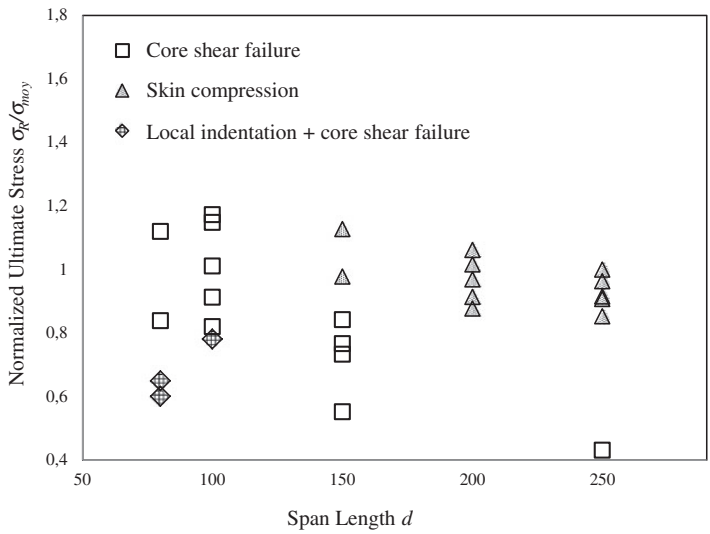

Figure 8. Experimental normalised ultimate stress and failure modes with respect to the span length.

decrease with the increase of the span length. Thus, for the shortest beams, the core shear failure stress strongly depends on the mechanical properties of the balsa wood block in which failure occurs. However, for the longest beam, the compressive strength of the Flax/Elium composites appears to be more stable. Nevertheless, the statistical spread observed is greatest for the particular span length $d = 150$ mm. In this case, core shear failure or skin compressive failure are randomly observed.

To understand that, a failure mode map corresponding to the $[0]_5$ sandwich eam was designed. This approach, described by Gibson and Triantafillou [36] for foam core sandwiches, consists in determining the transition equations between different possible failure modes. It has been adapted by various of authors for numerous loading cases [37,38]. Considering a general flexural load case, the maximum bending moment M and the maximum transverse load T can be expressed by [39]

$$|M| = k_M PL \text{ and } |T| = k_T P \tag{9}$$

where k_M and k_T depend on the boundary conditions. In three-point bending, $k_M = 1/4$ and $k_T = 1/2$. For a cellular core, with mechanical properties depending on its density, one can express its main mechanical properties as follows

$$\begin{aligned} E_c &= C_E \rho_c^n \\ G_c &= C_G \rho_c^n \\ \tau_c &= C_\tau \rho_c^m \end{aligned} \tag{10}$$

where C_E, C_G, C_τ, m and n can be determined experimentally. Then, the ultimate loads corresponding to the main failure modes existing for sandwich beams can be expressed

$$\text{Compressive failure of upper skin:} \quad P = \frac{\sigma_f t_f h}{k_M d} \tag{11}$$

$$\text{Core shear failure:} \quad P = \frac{C_\tau \rho_c^m h}{k_M d} \tag{12}$$

$$\text{Face buckling:} \quad P = \frac{t_f h}{2 k_M L} \sqrt[3]{E_f C_E C_G \rho_c^{2n}} \tag{13}$$

Equating these loads gives the transitions between these possible failure modes. For example, the transition between failure due to stretching or compression of the skin and core shear is given by

$$\log(\rho_c) = \frac{1}{m} \log \frac{\sigma_f k_T}{k_M C_\tau} \left(\frac{t_f}{d} \right) \tag{14}$$

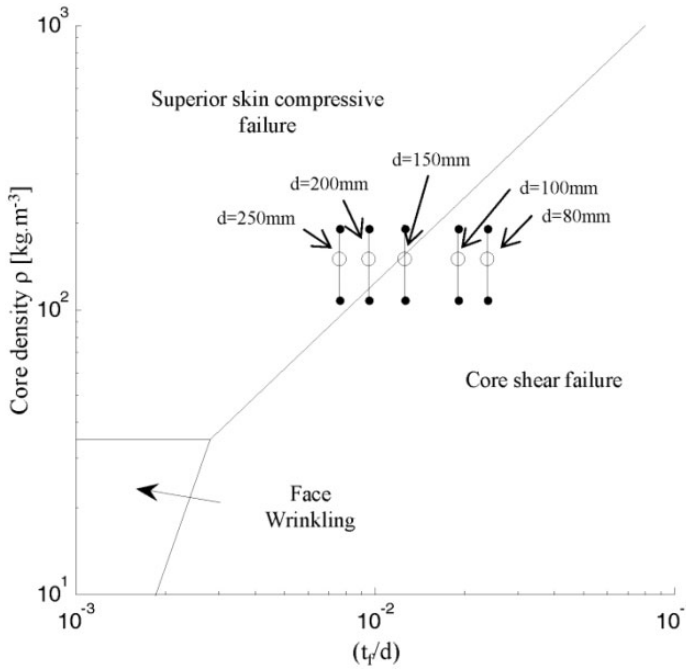

Figure 9. Failure mode map for $[0]_5$ specimens.

Thus, the failure modes map corresponding to a $[0]_5$ sandwich beam loaded in three-point bending is plotted in Figure 9. The experimental parameters used are given in Table 4. The material constants introduced in equation (10) were set as follows: $C_E = 0.35$, $C_G = 1.4$, $C_\tau = 0.02$ and $m = n = 1$, according to the experimental results proposed by Borrega et al. [21] and Da Silva et al. [22]. The different specimens tested experimentally were added to this map. The vertical bars represent the core density statistical dispersion, according to the Gaussian parameters measured in the 'Experimental program' section and with 95% of certainty. This analytical study confirms that for the particular span length $d = 150$ mm, the beam tested experimentally is located precisely at the border between core shear failure and compressive failure of the upper skins. One can conclude that both modes are observed randomly because of the dispersion of the core density, resulting in a dispersion of the core mechanical properties. In conclusion, this approach appears to be an efficient way for sizing such balsa wood cored sandwiches. The local variation of mechanical properties can be taken into account with the simple knowledge of the statistical dispersion of the balsa blocks' density. Higher accuracy in determining the failure mode borders could probably be achieved by considering the elastic and ultimate properties of balsa wood filled with Elium resin. However, this would require a considerable amount of experimental work.

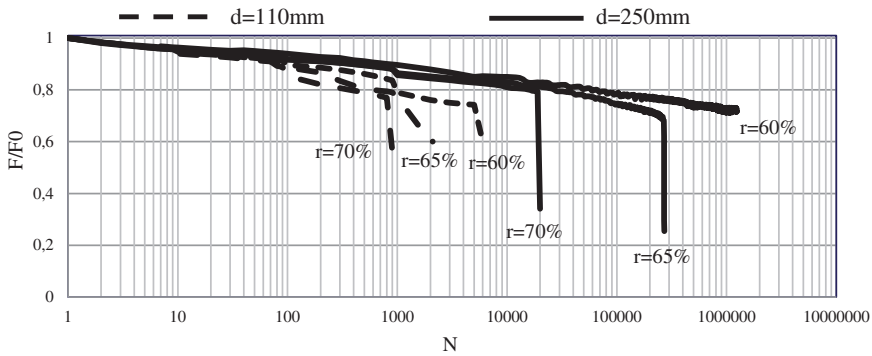

Figure 10. Evolution of the maximal load applied with the number of cycles for two different span lengths.

Fatigue properties

The fatigue flexural behaviour of $[0/90]_s$ Flax/Elium/Sandwich beams was also investigated. Fatigue tests were performed to determine the lifetime of this structure under different loading ratios and to compare this structure to GFRP/foam cored sandwiches. In this case, two different span lengths were used, $d = 110$ mm and $d = 250$ mm, in order to analyse the shear and flexural properties of the beams.

Fatigue behaviour

First, the evolution of the mechanical properties of the beams with the number of cycles was studied. Figure 10 presents typical evolutions of the maximum load F_{max} applied, with the number of cycles, normalised by the initial maximum load F_0, for both sets of specimens and for different loading ratios. In both cases, the F_{max}/F_0 ratio follows a semi-logarithmic linear decrease which can by expressed by

$$F_{max}/F_0 = 1 - B\log(N) \tag{15}$$

where B is the degradation rate and N the number of cycles. This corresponds to a rapid initial loss of mechanical properties during the first 100 cycles, followed by a progressive evolution of the damage mechanisms. This behaviour is commonly observed for sandwich structures with GFRP skins and foam cores [40,41]. It is worth noticing that whatever the loading ratio, the beams tested with $d = 110$ mm present a higher degradation rate and fail earlier than beams tested with a span length $d = 250$ mm. This indicates that this sandwich structure is more easily damaged under shear loadings. Failure modes of broken specimens were also analysed. As observed during the quasi-static flexural analysis presented in

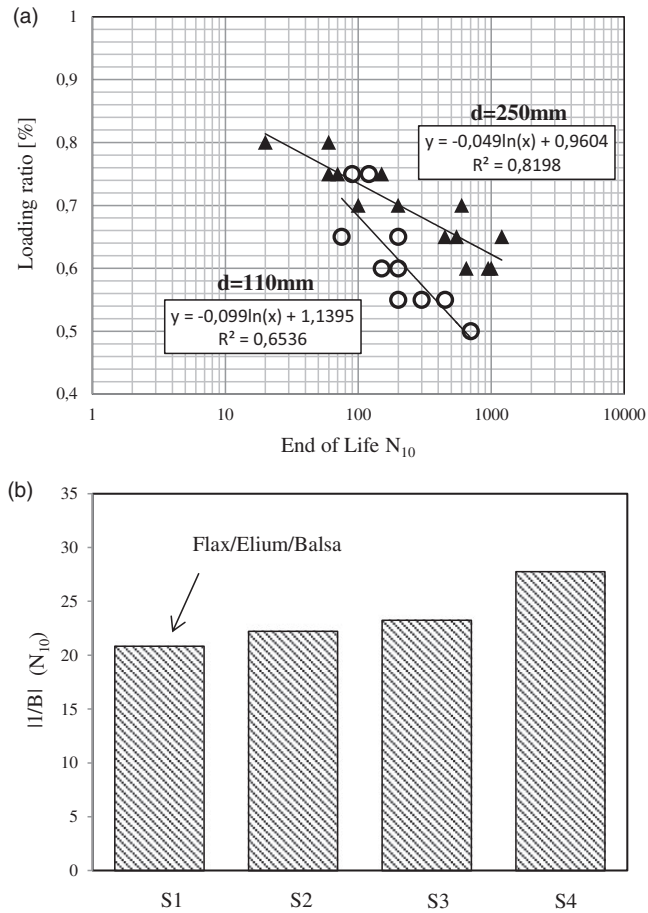

Figure 11. (a) Endurance diagram for $[0/90]_s$ sandwich beams and for two different span lengths; (b) fatigue performances of the Flax/Elium/Balsa sandwich compared to other non-bio-based materials.

the 'Quasi-static analysis' section, short beams exhibited core shear failure, whereas long beams presented compressive failure.

End-of-life analysis

For both sets of specimens, endurance diagrams were plotted to determine the end of life according to an N_{10} criterion for different loading ratios r. This criterion is satisfied when a 10% decrease in the maximum applied load is observed. Figure 11(a) presents the Wöhler diagrams corresponding to the span lengths $d = 110$ mm and $d = 250$ mm. In both cases, high scattering is observed. This can be explained by the randomness of fatigue failure. However, this scattering

Table 5. Geometrical and material properties of different sandwich beams.

Material	Fibres	Matrix	Core	e_p (mm)	e_a (mm)	ρ_a (kg/m3)	ϕ_{vf} (%)	Reference
S1	Flax	Elium	Balsa	1.6	15.9	150	35–40	Experimental
S2	Glass	Epoxy	PVC foam	1	15	200	~50	El Mahi et al.[43]
S3	Glass	Epoxy	PVC foam	1	15	100	~50	El Mahi et al.[43]
S4	Glass	Epoxy	PVC foam	3	15	200	~50	Assarar[42]

is more pronounced for short beams. As a matter of fact, the correlation coefficient r^2 appears to be 20% lower. The statistical spread of the mechanical properties of the core may explain this phenomenon. Moreover, the number of cycles to failure according to the N_{10} criterion appears smaller for short beams. The magnitude of the linear fitting's slope corresponding to the span length $d = 110$ mm is indeed 50% greater, indicating a higher degradation rate. This confirms that this material is more damaged when the core is subjected to shear loadings. Then, considering that the Wöhler curves can be fitted by an expression such as the one presented in equation (15), the value $|1/B|$ was used to compare the fatigue properties of the Flax/Elium/Balsa beams tested with a span length of 250 mm to those of non-bio-based beams tested in the same experimental conditions [42,43]. The geometrical and material properties of the sandwich beams considered are presented in Table 5. Figure 11(b) presents this comparison. The $|1/B|$ ratio is the smallest for the Flax/Elium/Balsa beams, indicating a higher degradation rate for this bio-based material. Nevertheless, the fatigue properties of these materials remain of a comparable order (less than 7% of difference compared to material B). Moreover, this difference could be offset by the potential mass reduction and reduced environmental impact of the Flax/Elium/Balsa sandwich material. This leads us to conclude that this material would be suitable for some applications as an additional option to GFRP/PVC foam cored sandwich structures.

Energy analysis

The previous experimental tests were used to study the energy dissipation capacity of this sandwich structure under different loading ratios. During the fatigue tests, the hysteresis cycles were analysed. Considering the hysteresis cycle illustrated in Figure 12, composed of $2n$ experimental points, one can express the maximum potential energy E_p applied to the system as

$$E_p = \frac{1}{2}\sum_{i=1}^{n}(d_{i+1} - d_i)(f(d_{i+1}) + f(d_i)) \tag{16}$$

This corresponds to the total area under the force–displacement curve corresponding to the loading phase of the hysteresis cycle. Moreover, the elastic energy

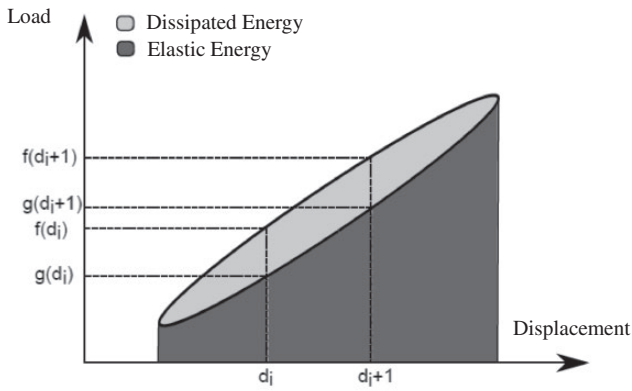

Figure 12. Illustration of a hysteresis cycle and its main parameters.

E_r is given by the area under the curve corresponding to the unloading phase which can be calculated by

$$E_r = \frac{1}{2}\sum_{i=1}^{n}(d_{i+1} - d_i)(g(d_{i+1}) + g(d_i)) \tag{17}$$

Thus, the energy dissipated by the material E_d and corresponding to the area of the hysteresis cycle is given by

$$E_d = E_p - E_r \tag{18}$$

Finally, the loss factor η is calculated by

$$\eta = \frac{E_d}{2\pi E_p} \tag{19}$$

Figure 13 presents the evolution of the fatigue loss factor η for the sandwich beams tested with a span length $d = 110$ mm and $d = 250$ mm, and for three different loading ratios r (60%, 65% and 70%). The results obtained for the span length $d = 110$ mm appear more scattered, probably due to local variations in the mechanical properties of the core. However, it is possible to conclude that the loss factor globally decreases with the increase in loading ratio. The opposite trend can be noticed for the span length $d = 250$ mm. These effects of the vibration amplitude and beam aspect ratio were also mentioned by Ganapathi et al. [44]. The authors performed numerical analyses on sandwich beams with different core properties and aspect ratios. They concluded that an increase in the amplitude of vibration

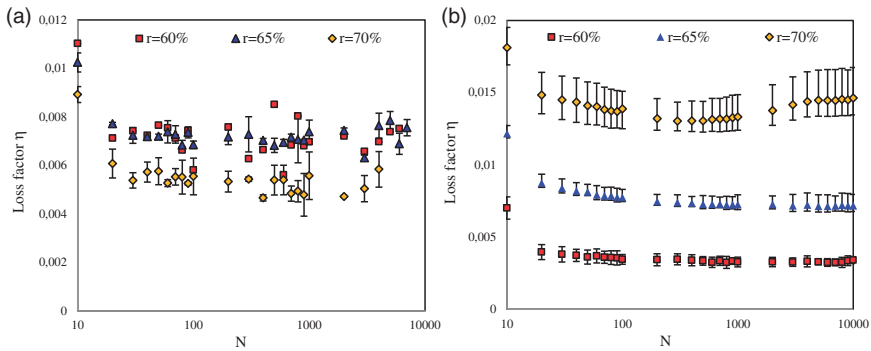

Figure 13. Evolution of the loss factor with the number of cycles and for different loading rations for the span lengths: (a) $d = 110$ mm; (b) $d = 250$ mm.

implies a decrease in the loss factor, which is much more pronounced for the smallest aspect ratios. However, for sandwich beams with higher core shear properties, the opposite tendency was observed for the higher aspect ratios.

For both span lengths, a similar evolution in the loss factor with the number of cycles can be seen. During the first hundred cycles, a rapid decrease in the loss factor can be observed whatever the loading configuration. For traditional cellular cored sandwich material, this phenomenon is often attributed to the first damage mechanisms in the core. Due to the appearance and propagation of microcracks, part of the air trapped in the cells is evacuated and no longer contributes to overall damping [45]. The loss factor evolution then becomes more stable for both span lengths. Finally, increasing trends can be noticed. This increase starts earlier for the higher loading ratios. It may be attributed to a global increase in the damage mechanisms, dissipating more energy due to friction phenomena. However, additional experimental investigations are required to fully understand the evolution of damages during fatigue tests. For example, acoustic emission technique could certainly provide additional information on the damage mechanisms occurring in the facings and in the core.

Conclusion

This work focuses on the experimental analysis of the static and dynamic flexural properties of a bio-based sandwich material made of thermoplastic skins reinforced by flax fibres and a balsa core. This structure is produced by a single-step liquid resin infusion process, an interesting perspective in the manufacturing of potentially recyclable bio-based composite structures. First, the quality of the skin/core interface was investigated. Flatwise tensile tests revealed good interfacial strength compared to existing GFRP/foam core sandwiches. This interesting property was attributed to the use of a low-viscosity resin with an open-cell balsa wood

core made of assembled elementary blocks. Preliminary analyses performed in the core revealed a dispersion of the mechanical properties described by a Gaussian law. In addition, quasi-static and cyclic three-point bending tests were performed to determine the elastic and ultimate properties of the skins and the core. Sandwich beams were tested with different span lengths in order to analyse the flexural and shear response of the structure. High scattering of the failure load was observed for a specific span length, corresponding to the transition between a core shear failure mode and a compressive failure mode of the upper skin. As a consequence, a failure mode map was designed based on existing theories and taking into account the dispersion of the mechanical properties of the core. This approach seems promising for sizing this kind of structure. In addition, the fatigue behaviour of this material was studied under three-point bending. The fatigue performances appear slightly lower than those of GFRP/foam cored sandwiches, but remain comparable. One can conclude that this material would be suitable for some semi-structural applications currently using GFRP/foam sandwich structures and subjected to fatigue loadings. The evolution of the loss factor with the number of cycles during fatigue cycles was also studied, revealing interesting damping properties for the first cycles. Additional experimental tests, involving non-destructive methods such as the acoustic emission technique, could probably help to determine more precisely the relation between damage evolution and loss factor evolution.

Acknowledgements

The authors thank Pierre Gerard and the ARKEMA company for their help with the processing of the Elium Resin.

Declaration of conflicting interests

The author(s) declared no potential conflicts of interest with respect to the research, authorship, and/or publication of this article.

Funding

The author(s) disclosed receipt of the following financial support for the research, authorship, and/or publication of this article: This study was supported by the MATIERES project and the "Région Pays de la Loire" in France.

References

1. Faruk O, Bledzki AK, Fink HP, et al. Biocomposites reinforced with natural fibers: 2000–2010. *Prog Polym Sci* 2012; 37: 1552–1596.
2. Satyanarayana KG, Arizaga GGC and Wypych F. Biodegradable composites based on lignocellulosic fibers - An overview. *Prog Polym Sci* 2009; 34: 982–1021.
3. Yan L, Chouw N and Jayaraman K. Flax fibre and its composites - A review. *Compos Part B: Eng* 2014; 56: 296–317.

4. Yan L, Kasal B and Huang L. A review of recent research on the use of cellulosic fibres, their fibre fabric reinforced cementitious, geo polymer and polymer composites in civil engineering. *Compos Part B: Eng* 2016; 92: 94–132.
5. Pil L, Bensadoun F, Pariset J, et al. Why are designers fascinated by flax and hemp fibre composites ? *Compos Part A: Appl Sci Manuf* 2016; 83: 193–205.
6. Wambua P, Ivens J and Verpoest I. Natural fibres : can they replace glass in fibre reinforced plastics ? *Compos Sci Technol* 2003; 63: 1259–1264.
7. Mancuso A, Pitarresi G and Tumino D. Mechanical behaviour of a green sandwich made of flax reinforced polymer facings and cork core. *Procedia Eng* 2015; 109: 144–153.
8. Castro O, Silva JM, Devezas T, et al. Cork agglomerates as an ideal core material in lightweight structures. *Mater Des* 2010; 31: 425–432.
9. Alcântara I, Teixeira-Dias F and Paulino M. Cork composites for the absorption of impact energy. *Compos Struct* 2013; 95: 16–27.
10. Fathi A, Wolff-Fabris F, Altstadt V, et al. An investigation on the flexural properties of balsa and polymer foam core sandwich structures: Influence of core type and contour finishing options. *J Sandw Struct Mater* 2013; 15: 487–508.
11. Grenestedt JL and Bekisli B. Analyses and preliminary tests of a balsa sandwich core with improved shear properties. *Int J Mech Sci* 2003; 45: 1327–1346.
12. Osei-Antwi M, De Castro J, Vassilopoulos AP, et al. Shear mechanical characterization of balsa wood as core material of composite sandwich panels. *Constr Build Mater* 2013; 41: 231–238.
13. Teles SV and Chimenti DE. Closed disbond detection in marine glass-epoxy/balsa composites. *NDT&E Int* 2008; 41: 129–136.
14. Le Duigou A, Deux J, Davies P, et al. PLLA flax mat balsa bio sandwich. Manufacture and mechanical properties. *Appl Compos Mater* 2011; 18: 421–438.
15. Karaduman Y and Onal L. Flexural behavior of commingled jute/polypropylene non-woven fabric reinforced sandwich composites. *Compos Part B: Eng* 2016; 93: 12–25.
16. Kandare E, Luangtriratana P and Kandola BK. Fire reaction properties of flax epoxy laminates and their balsa core sandwich composites with or without fire protection. *Compos Part B: Eng* 2014; 56: 602–610.
17. Sargianis JJ, Kim H-I, Andres E, et al. Sound and vibration damping characteristics in natural material based sandwich composites. *Compos Struct* 2013; 96: 538–544.
18. Monti A, El Mahi A, Jendli Z, et al. Experimental and finite elements analysis of the vibration behaviour of a bio-based composite sandwich beam. *Compos Part B: Eng* 2017; 110: 466–475.
19. Khalfallah M, Abbès B, Abbès F, et al. Innovative flax tapes reinforced Acrodur bio-composites: A new alternative for automotive applications. *Mater Des* 2014; 64: 116–126.
20. Boumbimba R, Coulibaly M, Khabouchi M, et al. Glass fibres reinforced acrylic thermoplastic resin-based tri-block copolymers composites : Low velocity impact response at various temperatures. *Compos Struct* 2017; 160: 939–951.
21. Borrega M and Gibson LJ. Mechanics of balsa (Ochroma pyramidale) wood. *Mech Mater* 2015; 84: 75–90.

22. Da Silva A and Kyriakides S. Compressive response and failure of balsa wood. *Int J Solids Struct* 2007; 44: 8685–8717.
23. Vural M and Ravichandran G. Dynamic response and energy dissipation characteristics of balsa wood : Experiment and analysis. *Int J Solids Struct* 2003; 40: 2147–2170.
24. Soden PD and Mcleish D. Variables affecting the strength of balsa wood. *J Strain Anal* 2015; 11: 225–234.
25. ASTM C297/C297M–04. *Standard test method for flatwise tensile strength of sandwich constructions*. West Conshohocken, PA: ASTM, 2004.
26. ASTM D7249/D7249M –06. *Standard test method for facing properties of sandwich constructions by long beam flexure*. West Conshohocken, PA: ASTM, 2006.
27. ASTM C393/C393M –16. *Standard test method for core shear properties of sandwich constructions by beam flexure*. West Conshohocken, PA: ASTM, 2016.
28. Liang S, Gning P and Guillaumat L. Properties evolution of flax epoxy composites under fatigue loading. *Int J Fatigue* 2014; 63: 36–45.
29. Haskell AB. *A durability and utility analysis of EFPI optic strain sensors embedded in composite materials for structural health monitoring*. Electronic Theses and Dissertations, Univeristy of Maine, USA, 2004.
30. Hou T-H, Baughman JM, Zimmerman TJ, et al. Evaluation of sandwich structure bonding in out-of-autoclave processing. *SAMPE J* 2010; 47.
31. Tuwair H, Hopkins M, Volz J, et al. Evaluation of sandwich panels with various polyurethane foam cores and ribs. *Compos Part B: Eng* 2015; 79: 262–276.
32. Correia JR, Garrido M, Gonilha JA, et al. GFRP sandwich panels with PU foams and PP honeycomb cores for civil engineering structural applications. *Int J Struct Integrity* 2012; 3: 127–147.
33. Sok T. *Effects of angled stitch reinforcement on foam core sandwich structures*. MSc Thesis, University of Utah, USA, 2012.
34. Monti A, El Mahi A, Jendli Z, et al. Mechanical behaviour and damage mechanisms analysis of a flax-fibre reinforced composite by acoustic emission. *Compos Part A: Appl Sci Manuf* 2016; 90: 100–110.
35. ASTM C273/C273M –16. *Standard test method for shear properties of sandwich core materials*. West Conshohocken, PA: ASTM, 2016.
36. Triantafillou TC and Gibson LJ. Failure mode maps for foam core sandwich beams. *Mater Sci Eng* 1987; 95: 37–53.
37. Andrews EW and Moussa NA. Failure mode maps for composite sandwich panels subjected to air blast loading. *Int J Impact Eng* 2009; 36: 418–425.
38. PabloFrancucci J, Xiong GJ and Stocchi A. Failure mode maps of natural and synthetic fiber reinforced composite sandwich panels. *Compos Part A: Appl Sci Manuf* 2017; 94: 217–225.
39. Zenkert D. *The handbook of sandwich construction*. Warrington, UK: EMAS Publishing, 1997.
40. Boukharouba W, Bezazi A and Scarpa F. Identification and prediction of cyclic fatigue behaviour in sandwich panels. *Measurement* 2014; 53: 161–170.
41. Ben Ammar I, Karra C, El Mahi A, et al. Mechanical behavior and acoustic emission technique for detecting damage in sandwich structures. *Appl Acoust* 2014; 86: 106–117.

42. Assarar M. *Etude expérimentale et modélisation du comportement dynamique des composites stratifiés et sandwichs*. Thesis, Université du Maine, France, 2007.
43. El Mahi A, Farooq MK, Sahraoui S, et al. Modelling the flexural behaviour of sandwich composite materials under cyclic loading. *Mater Des* 2004; 25: 199–208.
44. Ganapathi M, Patel BP, Boisse P, et al. Flexural loss factors of sandwich and laminated composite beams using linear and nonlinear dynamic analysis. *Compos Part B: Eng* 1999; 30: 245–256.
45. Idriss M, El Mahi A, Assarar M, et al. Damping analysis in cyclic fatigue loading of sandwich beams with debonding. *Compos Part B: Eng* 2013; 44: 597–603.